Study of Supramolecular Side-Chain and Cross-Linking Polymers by Complexation of Various H-Donor Acids with H-Acceptor Copolymers Containing Pendent Carbazole and Fluorescent Pyridyl Units

TZUNG-CHI LIANG, HONG-CHEU LIN

Department of Materials Science and Engineering, National Chiao Tung University, Hsinchu, Taiwan, Republic of China

Received 12 January 2009; accepted 19 February 2009
DOI: 10.1002/pola.23358
Published online in Wiley InterScience (www.interscience.wiley.com).

ABSTRACT: Two H-bonded acceptor (H-acceptor) homopolymers **14** and **17** were successfully prepared by polymerization of fluorescent pyridyl monomers **PBT** and **PBOT** (**12** and **13**), which were synthesized via Sonogashira coupling and Wittig-Horner reactions. To increase the glass transition temperatures as well as reduce the π-π stacking of the photoluminescent (PL) H-acceptor copolymers and their H-bonded polymer complexes, fluorescent monomers **12** and **13** were copolymerized with *N*-vinylcarbazole monomer **CAZ** (23) to produce H-acceptor copolymers **15–16** and **18–19**. Supramolecular side-chain and crosslinking polymers (i.e., H-bonded polymer complexes) obtained by complexation of light-emitting H-acceptor polymers **14–19** with various proton donor (H-donor) acids **20–22** were further characterized by DSC, POM, FTIR, XRD, and PL measurements. The mesomorphic properties can be tuned from the nematic phase in H-acceptor homopolymers (**14** and **17**) to the tilted smectic C phase in their H-bonded polymer complexes (**14/20–21** and **17/20–22**) by the introduction of H-donor acids (20–22). Moreover, the PL properties of light-emitting H-acceptor polymers can be adjusted not only by the central structures of the conjugated pyridyl cores but also by their surrounding nonfluorescent H-donor acids. In general, redder shifts of PL emissions in H-bonded polymer complexes occurred when the light-emitting H-acceptor polymers were complexed with H-donors having smaller pKa values. © 2009 Wiley Periodicals, Inc. J Polym Sci Part A: Polym Chem 47: 2734–2753, 2009

Keywords: conjucated polymers; fluorescence; liquid crystalline polymers (LCP); side-chain fluorescent polymers; supramolecular polymers; supramolecular structures

INTRODUCTION

Supramolecular chemistry is a new and exciting branch of chemistry encompassing systems held together by noncovalent bonds, and such complexes have considerable application potentials in the rapidly developing fields of molecular electronics and optoelectronics.[1,2] More recently, the concept of supramolecular chemistry has been applied to the design of liquid crystalline (LC) polymers in the expectation that molecular interactions may be amplified into macroscopically observable phenomena of self-assembled phases, that is, liquid crystallinity.[3] Supramolecular liquid crystals are molecular complexes generated from complexation of molecular species through

Correspondence to: H.-C. Lin (E-mail: linhc@mail.nctu.edu.tw)

Journal of Polymer Science: Part A: Polymer Chemistry, Vol. 47, 2734–2753 (2009)

noncovalent interactions, for example, hydrogen bonding. Kato et al. first exploited two different and independent components to generate liquid crystals through intermolecular hetero-hydrogen-bonding interaction, and this concept in turn resulted in numerous findings of such supramolecular liquid crystals.[4–9] The mesomorphic properties can be easily modified by miscellaneous proton donors and acceptors, and new LC properties, which are different from those of their original moieties, can be easily obtained by the introduction of supramolecular structures. Many kinds of H-bonds and building elements have been explored in the H-bonded structures to stabilize LC phases.[10–17] Therefore, side-chain LC polymers consisting of polymer backbones, flexible spacers, and mesogenic pendants have great potentials in various utilizations as novel technological materials, such as optical switching elements, optical storage devices, and information displays. Among these approaches, intermolecular H-bonding is simply acquired by complexation of H-bonded donor (H-donor) carboxylic (or benzoic) acid groups with H-bonded acceptor (H-acceptor) pyridyl moieties. Several series of H-bonded polymer complexes and side-chain LC polymers through intermolecular H-bonding (interaction between benzoic acid and pyridine) have been reported lately.[18–30]

The advantages of using organic materials to manufacture electroluminescent (EL) devices are their excellent film-forming properties, processing feasibilities of flexible devices, highly efficient EL properties, and low costs of fabrication.[31] As we know, poly(*N*-vinylcarbazole) (PVK) has attracted attention due to its applications related to polymer light-emitting diodes (PLEDs) in which the hole transporting layer is formed by PVK or it can be blended with other light-emitting materials. Such PLED devices have shown remarkably high luminescence efficiencies and relatively facile color tunabilities.[32–34] In contrast to PVK, Romero et al.[35] observed an increase in the external quantum efficiency of PLED devices based on the copolymerization of carbazole units with short thiophene segments, so carbazole units were also used to copolymerize with fluorescent pyridyl moieties in our study. Moreover, tuning emission colors in organic light-emitting materials have been established through the supramolecular interactions, for example, H-bonds, in organic, dendritic, and polymeric H-bonded complex systems.[36–38]

In this report, fluorescent pyridyl H-acceptors as pendent groups were incorporated into the side-chain polymeric structures rather than as small molecules in our previous studies.[36–38] The purpose of the present study for side-chain conjugated pyridyl polymers is to explore the self-assembled utilization of singly and doubly H-bonded structures (as shown in the schematic illustration of Fig. 1) in preparing for supramolecular side-chain and crosslinking polymers, respectively. As shown in Schemes 1 and 2, fluorescent H-acceptor monomers **PBT** and **PBOT** (**12** and **13**) and their corresponding H-acceptor homopolymers (**14** and **17**) containing three-conjugated aromatic rings (including two lateral substituted methyl and methoxy groups with one pyridyl terminus) were prepared, and both pyridyl H-acceptor monomers **12** and **13** were further reacted with different molar ratios of carbazole monomer **CAZ (23)** to produce copolymers **15–16** and **18–19**, respectively. Thus, the glass transition temperatures of the H-acceptor polymers can be controlled by the contents of pendent carbazole monomer **CAZ (23)** in H-acceptor polymers (**14–16** and **17–19**). In addition to the syntheses of such fluorescent H-acceptor monomers and polymers, two series of different H-acceptor polymers **PBT1-PBT3** (**14–16**) and **PBOT1-PBOT3** (**17–19**) were complexed with asymmetric monofunctional H-donors **OBA (20)** and **ONA (21)** as well as symmetric bifunctional H-donor **THDA (22**), respectively, (as shown in Fig. 2). By incorporating of H-acceptor polymers to H-donor acids with different pKa values, the light-emitting properties of the supramolecular polymer complexes can be easily adjusted. Singly/doubly H-bonded processes of side-chain/crosslinking H-bonded polymers were confirmed and investigated by means of their LC properties, X-ray diffraction (XRD) patterns, and photoluminescent (PL) properties.

EXPERIMENTAL

Materials

N-vinylcarbazole **CAZ** (**23**) was purchased from Aldrich Chemical Co. and used without further purification. Azobisisobutyronitrile (AIBN) was purchased from Kanto Chemical Co. and recrystallized from ethanol at 40 °C followed by drying in a vacuum oven. Proton donors OBA (**20**) and ONA (**21**) were identified as the required materials by ^{1}H and ^{13}C NMR spectroscopy and elementary analyses, which were reported in our previous

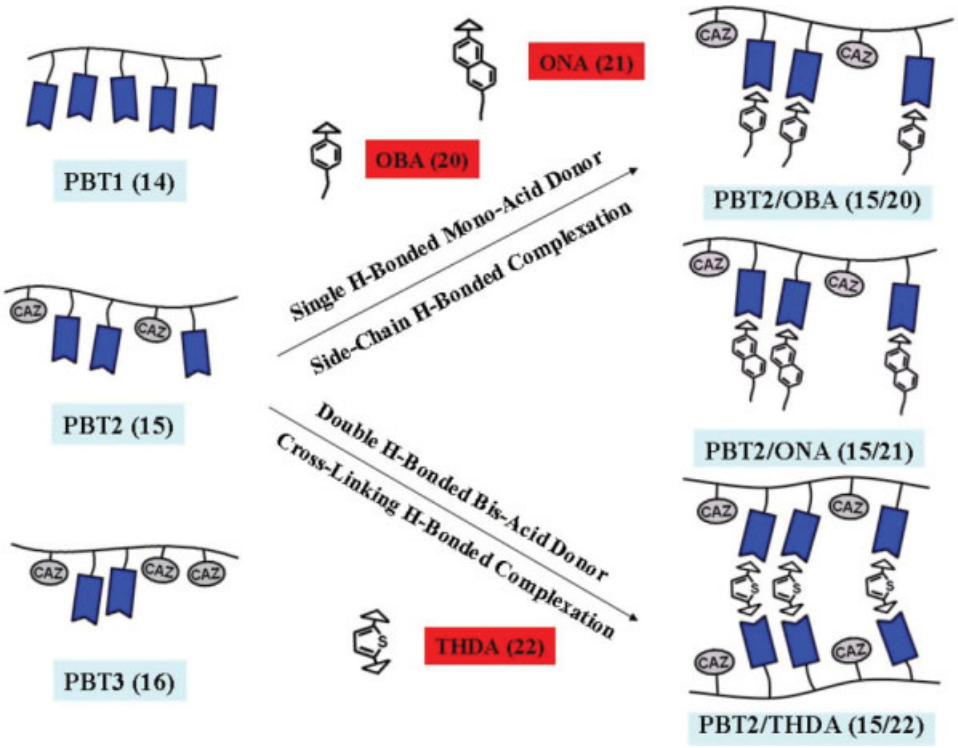

Figure 1. Schematic illustration of singly/doubly H-bonded processes for H-bonded side-chain/crosslinking polymers. [Color figure can be viewed in the online issue, which is available at www.interscience.wiley.com.]

results,[38] and proton donors thiophene-2,5-dicarboxylic acid **THDA** (**22**) was purchased from Aldrich Chemical Co. Chemicals and solvents were reagent grades and purchased from Aldrich, Acros, TCI, and Lancaster Chemical Co. Dichloromathane and Tetrahydrofuran (THF) were distilled to keep anhydrous before use. The other chemicals were used without further purification.

Syntheses of H-Acceptor Monomers PBT (12) and PBOT (13)

The synthetic route of monomer **PBT** (**12**) is shown in Scheme 1, and its synthetic procedures are described as follows:

4-Bromo-2,5-dimethylbenzaldehyde (2)

2,5-Dibromo-*p*-xylene 1 (6.9 g, 26.3 mmol) was dissolved in 60 mL of dry THF purged with nitrogen. A solution of *n*-BuLi (13.7 mL, 34.2 mmol, 2.5 M in hexane) was added dropwise to a rapidly stirred THF at −78 °C. The rate of addition was adjusted to keep the temperature below −78 °C. After the solution was stirred to react for 2 h at −78 °C, a solution of DMF (4.1 mL, 52.6 mmol) was added dropwise to keep at the same temperature. After 2 h, the reaction was quenched with water and extracted with ethyl acetate. The organic extracts were dried over Na_2SO_4, and then evaporated. The crude product was purified and recrystallized from *n*-hexane to give a white crystal. Yield: 5.0 g (90%).

^{1}H NMR (ppm, $CDCl_3$): δ 10.19 (s, 1H), 7.63 (s, 1H), 7.47 (s, 1H), 2.60 (s, 3H), 2.43 (s, 3H).

4-Bromo-2,5-dimethylbenyl Alcohol (3)

To a stirred solution of compound **2** (5.0 g, 23.7 mmol) in 100 mL of THF/MeOH (1:1), $NaBH_4$ (0.9 g, 23.7 mmol) was added very slowly and reacted at room temperature. After 1 h, the solution was cooled to 0 °C by ice bath, acidified with dilute HCl solution, and extracted with ethyl acetate. The resulting extracts in organic phase were combined and washed with water. Then, the organic extracts were dried over Na_2SO_4 and evaporated. The crude product was purified and recrystallized

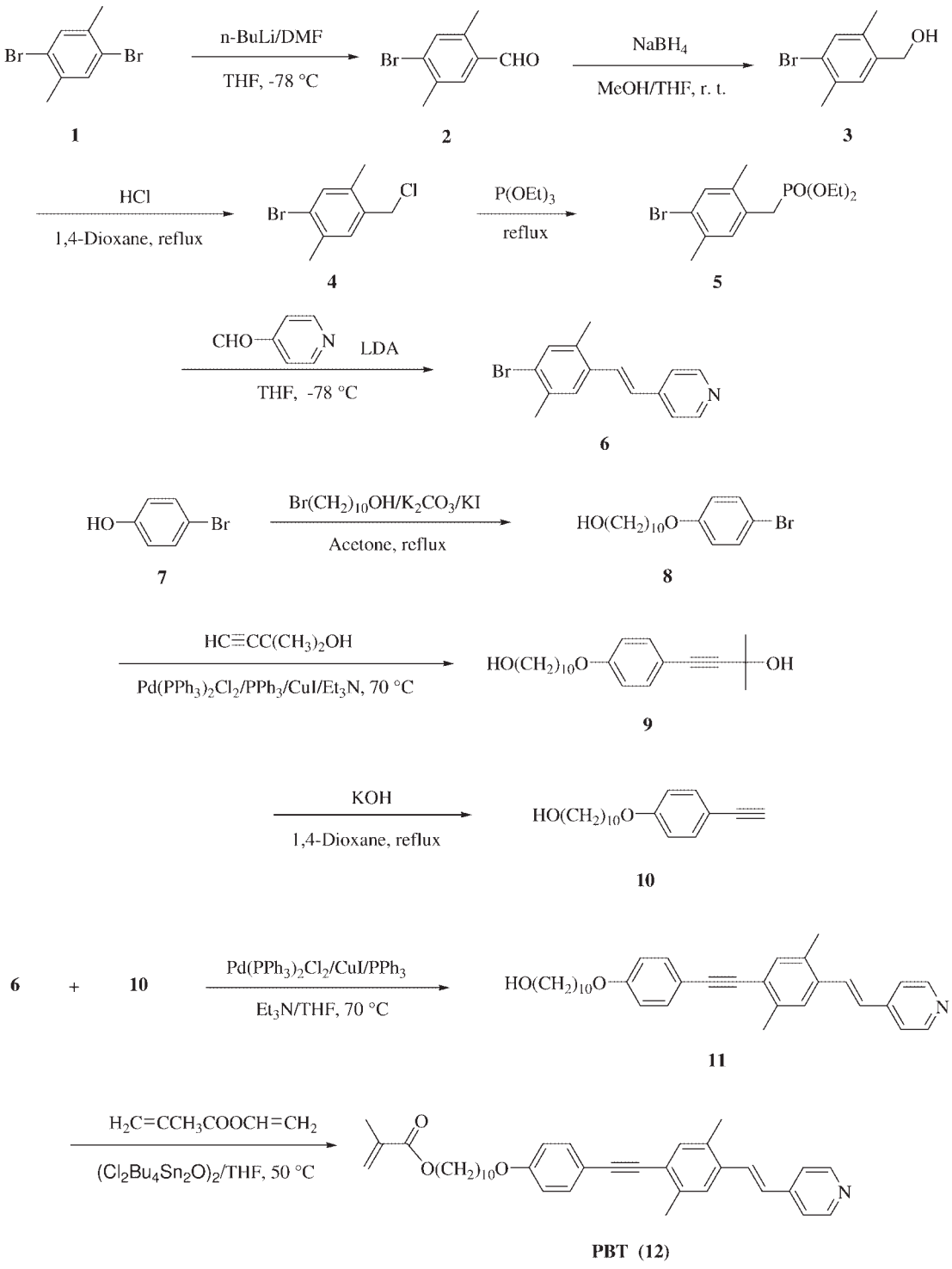

Scheme 1. Synthetic routes of monomer **PBT (12)**.

from dichloromethane/2-propanol to give a colorless crystal. Yield: 4.1 g (80%).

^{1}H NMR (ppm, $CDCl_3$): δ 7.33 (s, 1H), 7.21 (s, 1H), 4.61 (s, 2H), 2.35 (s, 3H), 2.27 (s, 3H).

1-Bromo-4-chloromethyl-2,5-dimethoxybenzene (4)

A stirred solution of compound **3** (4.1 g, 19 mmol) in 1,4-dioxane (150 mL) was added with

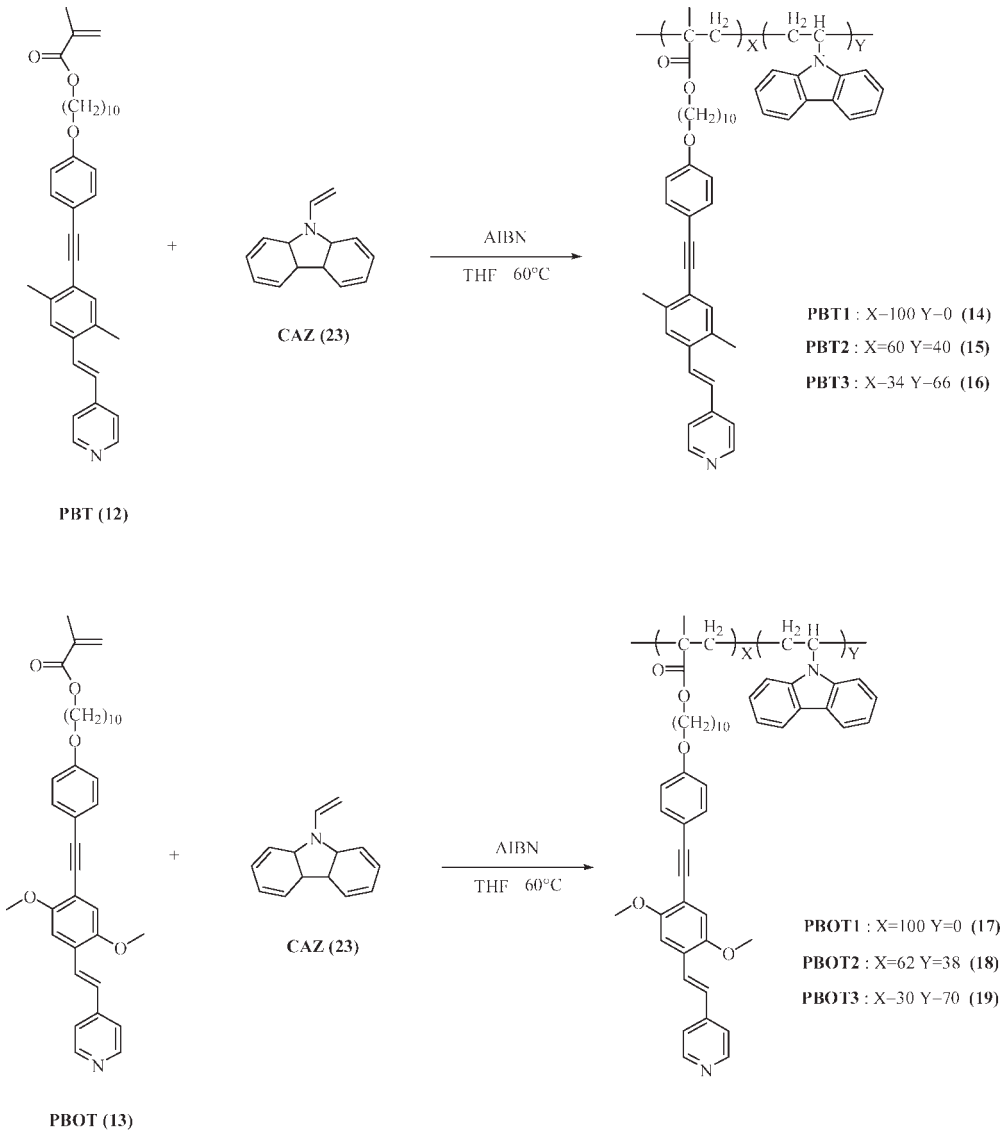

Scheme 2. Synthetic routes of H-acceptor polymers.

concentrated HCl (20 mL, 3 N), and then the mixture was refluxed for 10 h. After the reaction was completed, the crude mixture was added with water. The organic layer was extracted with ethyl acetate, dried over Na_2SO_4 and evaporated. The crude product was purified by flash column chromatography (silica gel, *n*-hexane/ethyl acetate 40:1) to give a white solid. Yield: 4.0 g (89%).

^{1}H NMR (ppm, $CDCl_3$): δ 7.36 (s, 1H), 7.15 (s, 1H), 4.51 (s, 2H), 2.36 (s, 6H).

4-Bromo-2,5-dimethylbenzyldiethylphosphonate (5)

Compound **4** (4.0 g, 17.1 mmol) was mixed with an excess of triethylphosphite (20 mL) and heated to reflux for 12 h under reduce pressure. The excess of triethylphosphite was removed after reaction. The crude product was purified and washed with hot hexane to give a white solid. Yield: 5.1 g (90%).

^{1}H NMR (ppm, $CDCl_3$): δ 7.28 (s, 1H), 7.07 (s, 1H), 4.08–3.95 (m, 10H), 3.06 (s, 1H), 2.99 (s, 1H), 2.28 (s, 3H), 2.26 (s, 3H).

1-Bromo-2,5-dimethyl-4-[2-(4-pyridyl) ethenyl]benzene (6)

Compound **5** (5.1 g, 15.1 mmol) was dissolved in 60 mL of dry THF purged with nitrogen. A solution of lithium diisopropylamide (22.7 mL,

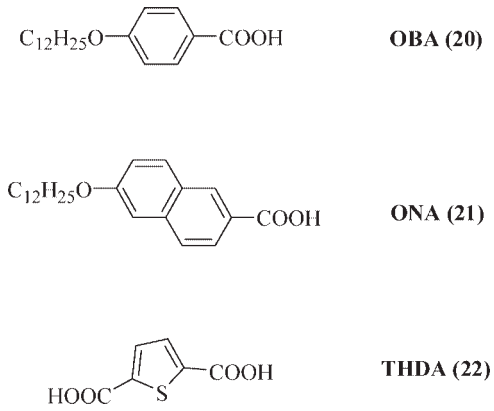

Figure 2. Mono-acid (singly H-bonded) and bisacid (doubly H-bonded) donors used in supramolecular side-chain/crosslinking polymers, respectively.

45.3 mmol, 2.5 M in hexane) was added dropwise to a rapidly stirred solution at −78 °C. The rate of addition was adjusted to maintain the temperature below −78 °C. After the solution was stirred to react for 30 min at −78 °C, a solution of pyridine-4-carboxaldehyde (2 mL, 21.1 mmol) was added dropwise and stirred for 30 min to come back to room temperature. After that, the mixture was stirred to react for 18 h at room temperature. The reaction was quenched with water and extracted with dichloromethane. Subsequently, the organic layer was dried over Na_2SO_4 and evaporated. The crude product was purified by column chromatography (silica gel, dichloromethane/acetone 20:1) to give a yellow solid. Yield: 3.7 g (85%).

^{1}H NMR (ppm, $CDCl_3$): δ 8.56 (d, J = 4.8 Hz, 2H), 7.42 (s, 1H), 7.40 (d, J = 16.2 Hz, 1H), 7.36 (s, 1H), 7.35 (d, J = 4.8 Hz, 2H), 6.88 (d, J = 16.2 Hz, 1H), 2.38 (s, 3H), 2.35 (s, 3H).

10-(4-Bromophenoxy)-decan-1-ol (8)

A mixture of 4-bromophenol **7** (4.9 g, 28.5 mmol), potassium carbonate (8.7 g, 62.7 mmol), 10-bromodecanol (7.4 g, 31.4 mmol), and a few amount of potassium iodide in acetone (200 mL) was heated to reflux and stirred under nitrogen for 48 h. After cooling to room temperature, the solvent was removed under reduced pressure. The residue was taken up in water and extracted with ethyl acetate. Then, the organic layer was dried over Na_2SO_4 and evaporated. The crude product was purified by column chromatography (silica gel, *n*-hexane/ethyl acetate 3:1) to give a white solid. Yield: 8.3 g (88%).

^{1}H NMR (ppm, $CDCl_3$): δ 7.33 (d, J = 9.0 Hz, 2H), 6.75 (d, J = 9.0 Hz, 2H), 3.89 (t, J = 6.3 Hz, 2H), 3.62 (t, J = 6.6 Hz, 2H), 1.78–1.69 (m, 2H), 1.59–1.50 (m, 2H), 1.41–1.29 (m, 12H).

4-[4-(10-Hydroxy-decyloxy)-phenyl]-2-methyl-3-butyn-2-ol (9)

A solution of compound **8** (8.3 g, 25.3 mmol), PPh_3 (13.1 mg, 0.51 mmol), and CuI (73 mg, 0.38 mmol) in dry triethylamine (80 mL) was degassed with nitrogen for 5 min. 2-Methyl-3-butyn-2-ol (3.7 mL, 38 mmol) and $Pd(PPh_3)_2Cl_2$ (180 mg, 0.25 mmol) were added to the solution at room temperature and the mixture was stirred to react at 70 °C for 12 h. The mixture was filtered and the solvent was removed in vacuum. Afterward, the crude mixture was extracted using dichloromethane. The organic solution was washed with water, and then dried over Na_2SO_4 and evaporated. The crude product was followed by purifying with column chromatography (silica gel, *n*-hexane/ethyl acetate 2:1) to give a light yellow solid. Yield: 4.7 g (56%).

^{1}H NMR (ppm, $CDCl_3$): δ 7.31 (d, J = 9.0 Hz, 2H), 6.79 (d, J = 9.0 Hz, 2H), 3.92 (t, J = 6.6 Hz, 2H), 3.62 (t, J = 6.6 Hz, 2H), 1.77–1.70 (m, 2H), 1.60 (s, 6H), 1.58–1.50 (m, 2H), 1.42–1.29 (m, 12H).

4-Ethynyl-1-(10-hydroxydecan-1-yloxy)-benzene (10)

A solution of compound **9** (4.7 g, 14.2 mmol) and finely powdered KOH (2.39 g, 42.6 mmol) in 1,4-dioxane (80 mL) was refluxed under nitrogen for 3 h. After cooling to room temperature, the solvent was removed under reduced pressure. The residue was taken up in water and extracted with ethyl acetate, and then acidified with 150 mL of HCl (3 N). The organic solution was washed with water, and then dried over Na_2SO_4 and evaporated. The crude product was purified by column chromatography (silica gel, *n*-hexane/ethyl acetate 4:1) to give a light yellow solid. Yield: 3.6 g (92%).

^{1}H NMR (ppm, $CDCl_3$): δ 7.39 (d, J = 9.0 Hz, 2H), 6.80 (d, J = 9.0 Hz, 2H), 3.92 (t, J = 6.6 Hz, 2H), 3.62 (t, J = 6.6 Hz, 2H), 2.97 (s, 1H), 1.80–1.70 (m, 2H), 1.57–1.50 (m, 2H), 1.42–1.29 (m, 12H).

10-{4-[2,5-Dimethyl-4-(2-pyridin-4-yl-vinyl)-phenylethynyl]-phenoxy}-decan-1-ol (11)

A mixture of compound **6** (3.7 g, 12.7 mmol), PPh_3 (170 mg, 0.64 mmol), and CuI (120 mg,

0.64 mmol) in dry triethylamine (80 mL) was degassed with nitrogen for 5 min. Compound **10** (3.6 mL, 13.3 mmol) and $Pd(PPh_3)_2Cl_2$ (90 mg, 0.13 mmol) were added to the solution at room temperature, and afterward the reaction mixture was stirred to react at 70 °C for 12 h. The mixture was filtered and the solvent was removed in vacuum. Next, the crude mixture was extracted using dichloromethane. The organic solution was washed with water, and then dried over Na_2SO_4 and evaporated. The crude product was purified by column chromatography (silica gel, dichloromethane) to give a light yellow solid. Yield: 4.4 g (72%).

^{1}H NMR (ppm, $CDCl_3$): δ 8.61 (d, J = 6.0 Hz, 2H), 7.56 (d, J = 15.9 Hz, 1H), 7.51 (s, 1H), 7.49 (d, J = 8.7 Hz, 2H), 7.44 (d, J = 6.0 Hz, 2H), 7.36 (s, 1H), 6.98 (d, J = 15.9 Hz, 1H), 6.90 (d, J = 8.7 Hz, 2H), 4.00 (t, J = 6.6 Hz, 2H), 3.68 (t, J = 6.6 Hz, 2H), 2.53 (s, 3H), 2.44 (s, 3H), 1.82 (m, 2H), 1.60 (m, 2H), 1.49–1.16 (m, 12H).

2-Methyl-acrylic acid 10-{4-[2,5-dimethyl-4-(2-pyridin-4-yl-vinyl)-phenylethynyl]-phenoxy}-decyl Ester PBT (12)

Compound 11 (1.0 g, 2.1 mmol), vinyl methacrylate (1.24 mL, 0.01 mmol), 1,3-dichloro-1,1,3,3-tetrabutyldistannoxane (92 mg, 0.83 mmmol), 2,6-di-*tert*-butyl-4-methyl phenol (27 mg, 1.3 mmmol), and 2 mL of THF were added to a round-bottom flask. The solution was stirred at 50 °C for 48 h. Finally, the crude product of monomer **PBT (12)** was purified by column chromatography (aluminum oxide, *n*-hexane/dichloromethane 4:1) to give a light yellow solid. Yield: 0.54 g (47%).

^{1}H NMR (ppm, $CDCl_3$): δ 8.57 (d, J = 5.4 Hz, 2H), 7.51 (d, J = 16.2 Hz, 1H), 7.46 (s, 1H), 7.44 (d, J = 8.7 Hz, 2H), 7.39 (d, J = 5.4 Hz, 2H), 7.31 (s, 1H), 6.93 (d, J = 16.2 Hz, 1H), 6.85 (d, J = 8.7 Hz, 2H), 6.08 (s, 1H), 5.53 (s, 1H), 4.12 (t, J = 6.9 Hz, 2H), 3.96 (t, J = 6.9 Hz, 2H), 2.49 (s, 3H), 2.39 (s, 3H), 1.93 (s, 3H), 1.77 (m, 2H), 1.65 (m, 2H), 1.49–1.20 (m, 12H). ^{13}C NMR (ppm, $CDCl_3$): δ 159.30, 149.92, 145.09, 137.62, 134.60, 133.63, 133.60, 132.96, 130.52, 127.20, 126.47, 125.20, 123.72, 121.00, 115.30, 114.59, 94.65, 87.04, 77.52, 77.10, 76.67, 68.09, 64.84, 29.49, 29.46, 29.37, 29.25, 29.21, 28.62, 26.03, 25.99, 20.39, 19.20, 18.37. MS (EI): m/z [M^+] 549.3, calcd m/z [M^+] 549.32. Anal. Calcd. for $C_{37}H_{43}NO_3$: C 80.84, H 7.88, N 2.55. Found: C 80.56, H 7.95, N 2.77.

1-{[4-(10-Methacryloyloxy-decyloxy)-phenyl]-ethynyl}-2,5-dimethoxy-4-[2-(4-pyridyl)ethenyl]-benzene PBOT (13)

The synthetic procedures of monomer **PBOT (13)** were described in our previous report.[39]

^{1}H NMR (ppm, $CDCl_3$): δ 8.57 (d, J = 4.5 Hz, 2H), 7.66 (d, J = 16.5 Hz, 1H), 7.50 (d, J = 9.0 Hz, 2H), 7.39 (d, J = 4.5 Hz, 2H), 7.11 (s, 1H), 7.04 (d, J = 16.5 Hz, 1H), 7.04 (s, 1H), 6.87 (d, J = 9.0 Hz, 2H), 6.10 (s, 1H), 5.55 (s, 1H), 4.14 (t, J = 6.6 Hz, 2H), 3.97 (t, J = 6.6 Hz, 2H), 3.96 (s, 3H), 3.89 (s, 3H), 3.62 (t, J = 6.6 Hz, 2H), 1.95 (s, 3H), 1.81-1.75 (m, 2H), 1.58–1.53 (m, 2H), 1.42–1.30 (m, 12H). HRMS (EI): calcd for $C_{37}H_{43}NO_5$, 581.3141; found 581.3146. Anal. Calcd for $C_{37}H_{43}NO_5$: C, 76.39; H, 7.45; N, 2.41. Found: C, 76.15; H, 7.37; N, 2.44.

Syntheses of Polymers

The synthetic routes of polymers are shown in Scheme 2.

Homopolymers of PBT1 (14) and PBOT1 (17)

Monomers (1.0 g) of **PBT (12)** and **PBOT (13)** were dissolved in THF (5 mL), and then AIBN (3 mol %) was added as an initiator. After 24 h of reaction, the polymerization was terminated and the polymers were precipitated by a large amount of ether. The crude products were redissolved several times in THF and reprecipitated into a large amount of ether to afford 0.56 g of polymers. The yields were 65∼49%.

Copolymers PBT2-PBT3 (15–16) and PBOT2-PBOT3 (18–19)

Monomers (total amount 1.2 g) of **PBT (12)/CAZ (23)** or **PBOT (13)/CAZ (23)** with the desired molar ratios were dissolved in THF (6 mL), and then AIBN (3 mol %) was added as an initiator. The reaction mixtures were flushed with nitrogen for 5 min and then heated in a water bath at 60 °C to initiate polymerization. After 24 h of reaction, the polymerization was terminated and the copolymers were precipitated by a large amount of ether. The products were redissolved several times in THF and reprecipited in ether.

PBT1 (14)

Yield: 49%. ^{1}H NMR (ppm, *d*-dioxane): δ 0.89–1.75 (b, 18H), 1.93 (s, 3H), 2.33 (s, 3H), 2.46 (s,

3H), 3.84–4.03 (b, 4H), 6.78–7.61 (m, 10H), 8.51 (s, 2H).

PBT2 (15)

Yield: 55%. ^{1}H NMR (ppm, *d*-dioxane): δ 0.88–1.85 (b, 19H), 1.95 (s, 3H), 2.34 (s, 3H), 2.48 (s, 3H), 3.80–4.03 (b, 4H), 6.81–8.20 (m, 18H), 8.51 (s, 2H).

PBT3 (16)

Yield: 50%. ^{1}H NMR (ppm, *d*-dioxane): δ 0.92–1.88 (b, 19H), 1.96 (s, 3H), 2.36 (s, 3H), 2.49 (s, 3H), 3.80–4.05 (b, 4H), 6.82–8.22 (m, 18H), 8.53 (s, 2H).

PBOT1 (17)

Yield: 58%. ^{1}H NMR (ppm, *d*-dioxane): δ 0.88–1.78 (b, 18H), 2.08 (s, 3H), 3.79–4.02 (m, 10H), 6.79–7.78 (m, 10H), 8.50 (s, 2H).

PBOT2 (18)

Yield: 62%. ^{1}H NMR (ppm, *d*-dioxane): δ 0.90–1.83 (b, 19H), 2.10 (s, 3H), 3.80–4.05 (m, 10H), 6.78–8.19 (m, 18H), 8.50 (s, 2H).

PBOT3 (19)

Yield: 65%. ^{1}H NMR (ppm, *d*-dioxane): δ 0.87–1.85 (b, 19H), 2.16 (s, 3H), 3.83–4.10 (m, 10H), 6.65–8.21 (m, 18H), 8.51 (s, 2H).

Preparation of Supramolecular Complexes

In all cases, all proton donors (as shown in Fig. 2) and acceptor polymers were dissolved in THF to make a clear solution. After that, most of the solvents were evaporated under ambient conditions, which were followed by drying in a vacuum oven at 60 °C for several hours. The complexation of H-donor acids and H-acceptor polymers through hydrogen bonding occurred during the solvent evaporation. The complexes of all H-acceptor polymers with H-donor acids **OBA (20)** and **ONA (21)** had the equal molar amount of pyridyl H-acceptor and carboxylic acid H-donor groups (in 1:1 M ratio) to form singly H-bonded supramolecules (H-bonded side-chain polymers), and with **THDA (22)** had the double amounts of pyridyl H-acceptor groups to those of carboxylic acid H-donor groups (in 2:1 M ratio) to form doubly H-bonded supramolecules (H-bonded crosslinking polymers).

Measurements and Characterization

^{1}H NMR spectra were recorded on a Varian unity 300 MHz spectrometer using $CDCl_3$ and *d*-dioxane as solvents. Elemental analyses were performed on a HERAEUS CHN-OS RAPID elemental analyzer. Fourier transform infrared (FT-IR) spectra were performed a Nicolet 360 FT-IR spectrometer. The textures of mesophases were characterized by a polarizing optical microscope (POM, model: Leica DMLP) equipped with a hot stage. Temperatures and enthalpies of phase transitions were determined by differential scanning calorimetry (DSC, model: Perkin-Elmer Pyris 7) at the second heating and cooling scans with a rate of 10 °C/min under nitrogen. Thermogravimetric analyses (TGA) were conducted on a Du Pont Thermal Analyst 2100 system with a TGA 2950 thermogravimetric analyzer at a heating rate of 20 °C/min under nitrogen. Gel permeation chromatography (GPC) analyses were conducted with a Water 1515 separations module using polystyrene as a standard and THF as an eluant. UV-visible absorption spectra were recorded in dilute THF solutions (10^{-6} M) on a HP G1103A spectrophotometer, and photoluminescence (PL) spectra were obtained on a Hitachi F-4500 spectrophotometer. Thin films of UV-vis and PL measurements were spin-coated on quartz substrates from THF solutions with a concentration of 1 wt %. The PL quantum yields (Φ_{PL}) of polymers were measured with 9,10-diphenylanthracene as a reference (in cyclohexane, Φ_{PL} = 0.9).[40] Synchrotron powder XRD measurements were performed at beamline BL17A of the National Synchrotron Radiation Research Center (NSRRC) in Taiwan, where the X-ray wavelength used was 1.32633 Å. X-ray diffraction XRD data were collected using imaging plates (IP, of an area = 20 × 40 cm^2 and a pixel resolution of 100) curved with a radius equivalent to the sample-to-image plate distance of 280 mm, and the diffraction signals were accumulated for 3 min. The powder samples were packed into a capillary tube and heated by a heat gun, where the temperature controller was programmable by a PC with a PID feed back system. The scattering angle theta values were calibrated by a mixture of silver behenate and silicon.

Table 1. Molecular Weights and Thermal Properties of H-Acceptor Polymers

H-Acceptor Polymer	Composition (% **CAZ**)[a]	M_n[b]	M_w[b]	PDI[b]	T_d[c] (°C)	Phase Transitions[d] (°C)
PBT1 (14)	0	8,800	20,400	2.31	389	G 51 N[e]
PBT2 (15)	40	12,200	32,100	2.63	373	G 63 N[e]
PBT3 (16)	66	9,200	13,600	1.47	359	G 130 K[e]
PBOT1 (17)	0	10,100	20,100	1.99	362	G 61 N[e]
PBOT2 (18)	38	9,700	19,100	1.96	341	G 70 N[e]
PBOT3 (19)	70	15,000	44,000	2.93	335	G 103 K[e]

[a] The content of **CAZ** groups in copolymers (mol %) were determined by NMR.
[b] Molecular weight determined was by GPC in THF, based on polystyrene standards.
[c] Temperature (°C) at 5% weight loss was measured by TGA at a heating rate of 20 °C/min under nitrogen.
[d] Glass transition temperature (°C) was determined by DSC at the second heating scan with a rate of 10 °C/min. G, glassy state; K, crystalline; N, nematic.
[e] The isotropization temperatures were not observed in DSC even up to 250 °C.

RESULTS AND DISCUSSION

Synthesis and Characterization of Polymers

As shown in Scheme 1, monomer **PBT (12)** was successfully synthesized via Sonogashira coupling and Wittig-Horner reactions to obtain three-conjugated aromatic rings. To synthesize the designed methacrylate monomer containing end-capping pyridine, it is crucial to avoid H-bonding of the pyridine moiety, and thus no acidic reactants can be used. Therefore, vinyl methacrylate (instead of methacryloyl chloride) was finally used as a reactant according to the literature[41] to get a high yield of methacrylate **PBT (12)**, where 1,3-dichloro-1,1,3,3-tetrabutyldistannoxane was required as a catalyst to proceed this reaction and the polymerization of PBT was avoided by using an inhibitor 2,6-di-*tert*-butyl-4-methyl phenol. Two analogous series side-chain polymers composed of monomers **PBT (12)** and **PBOT (13)** with different lateral methyl and methoxy groups in central cores were synthesized. Finally, methacrylate monomers **PBT (12)** and **PBOT (13)** were in conjunction with *N*-vinylcarbazole **CAZ (23)** during the conventional synthesis of random free radical copolymerization, where the contents of **CAZ** units in the copolymers were determined by ^{1}H NMR. All of these polymers were dissolved in high polar organic solvents (such as THF and DMF) to form good transparent films on glass substrates. The average molecular weights obtained from GPC are illustrated in Table 1. The number-average molecular weights (M_n) of polymers are between 8800 and 15,000 g/mol with polydispersity indexes (PDI) between 1.47 and 2.93.

FT-IR Spectroscopy of H-Bonded Polymer Complexes

All H-bonded polymer complexes consisting of appropriate (fully H-bonded) molar ratios of H-acceptor polymers (**14–19**) and H-donors (**20–22**) were prepared by slow evaporation of THF solutions and followed by drying in vacuo. The formation of hydrogen bonding in supramolecular side-chain and crosslinking polymers containing donors **OBA (20), ONA (21)**, and **THDA (22)** was confirmed by FT-IR spectroscopy. As shown in Figure 3, IR spectra of **PBOT2 (18)**, **THDA (22)**, and H-bonded polymer complex **PBOT2/THDA (18/22)** are compared with analyze the hydrogen bonds in the supramolecular crosslinking structure of **PBOT2/THDA (18/22)**. In contrast to the O—H band of pure **THDA (22)** (H-bonded cross-

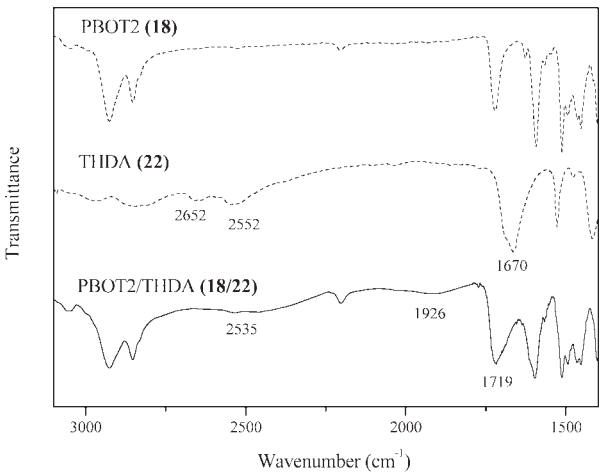

Figure 3. Infrared spectra for **PBOT2 (18)**, **THDA (22)**, and H-bonded polymer complex **PBOT2/THDA (18/22)** at room temperature.

linker) at 2652 and 2552 cm^{-1}, the weaker O—H band observed at 2535 and 1926 cm^{-1} in H-bonded polymer complex **PBOT2/THDA (18/22)** is indicative of stronger hydrogen bonding between the pyridyl group of **PBOT2 (18)** and the carboxylic acid of **THDA (22**) in the H-bonded polymer complex. On the other hand, a C=O stretching vibration appeared at 1719 cm^{-1} in H-bonded polymer complex **PBOT2/THDA (18/22)**, which shows that the carbonyl group was in a less associated state than that in pure **THDA (22)** (H-bonded cross-linker) with a weaker C=O stretching vibration appeared at 1670 cm^{-1}. Both results suggest that hydrogen bonds were formed between H-acceptor **PBOT2 (18)** and H-donor **THDA (22)** in the solid state of H-bonded polymer complex **PBOT2/THDA (18/22)**. Some other supramolecular polymers also have the similar consequences of H-bonding formation as the H-bonded polymer complex demonstrated here.[42]

Thermal Behavior

The phase transition temperatures and corresponding enthalpy changes of all polymers and H-bonded polymer complexes were characterized by DSC and POM, where the mesomorphic properties (the nematic and Sc phases) were affected by the type of H-donor acids and H-acceptor pyridyl polymers (containing lateral methyl- and methoxy-substituted groups). The thermal stabilities of the polymers evaluated by TGA under nitrogen are summarized in Table 1. TGA analyses indicate that the degradation temperatures (T_d) with 5% of weight loss under nitrogen are between 335 and 389 °C. The results of TGA show that the T_d values of the polymers are gradually decreased by increasing the molar ratio of the **CAZ** units in both series of polymers **PBT1-PBT3 (14–16)** and **PBOT1-PBOT3 (17–19**). In addition, lateral methyl-substituted polymers **PBT1-PBT3 (14–16**) have higher T_d values than analogous lateral methoxy-substituted polymers **PBOT1-PBOT3 (17–19**), respectively. The glass transition temperatures (T_g) of the polymers determined by DSC under nitrogen are also listed in Table 1. The glass transition temperatures of all polymers are between 51 and 130 °C, whereas their isotropization temperatures were not observed up to 250 °C. As shown in Figure 4, the T_g values of the polymers are gradually enhanced by increasing the molar ratio of the **CAZ** units, that is, **PBT3 (16)** > **PBT2 (15)** > **PBT1 (14)** and **PBOT3 (19)** > **PBOT2 (18)** > **PBOT1 (17**).

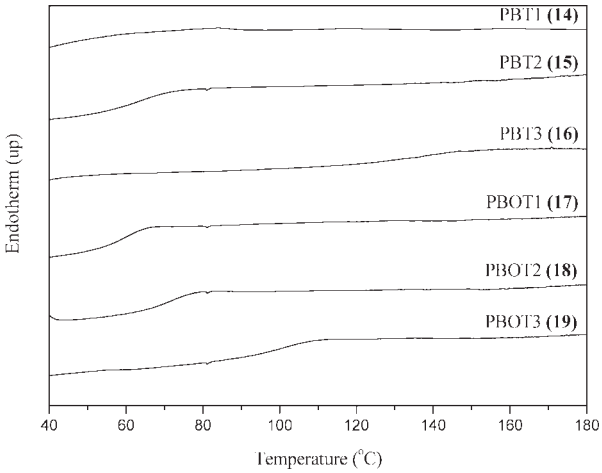

Figure 4. DSC heating curves (second scans) of H-acceptor polymers **14–19**.

This obviously indicates that the presence of the bulky and rigid **CAZ** moieties in the copolymers will enhance the steric hindrance of the pendants and suppresses the free volume of the copolymers effectively. Generally, the lateral methoxy-substituted polymers show higher glassy transition temperatures (T_g) than the corresponding methyl-substituted polymers, which might be because the higher polarity of the lateral methoxy groups in the H-acceptor pyridyl pendants may stabilize the frozen smectic layered structure by the succeeding mesophasic arrangement. As for the phase behavior of polymers **PBT1-PBT3 (14–16)** and **PBOT1-PBOT3 (17–19)** shown in Table 1, it suggests that the incorporation of **CAZ** units in copolymers **(14–19)** is detrimental to the formation of the nematic phase, so copolymers **PBT3 (16)** and **PBOT3 (19)** with the highest concentration of **CAZ** units (ca. 70% molar ratio) do not possess any mesophase in both series. This phenomenon could be explained by that the **CAZ** units with nonmesomorphic property may dilute and hinder the molecular packing of the LC arrangements.

All H-bonded polymer complexes consisting of appropriate (fully H-bonded) molar ratios of H-acceptors (polymers) and H-donors were prepared by slow evaporation of THF solutions and followed by drying in vacuo. The thermal properties of all H-bonded polymer complexes are illustrated in Figure 5 and Table 2. Similar to polymers **PBT1-PBT3 (14–16)** and **PBOT1-PBOT3 (17–19)**, the phase transition temperatures of these H-bonded polymer complexes have the same tendency. To investigate the effects of H-donors to form various

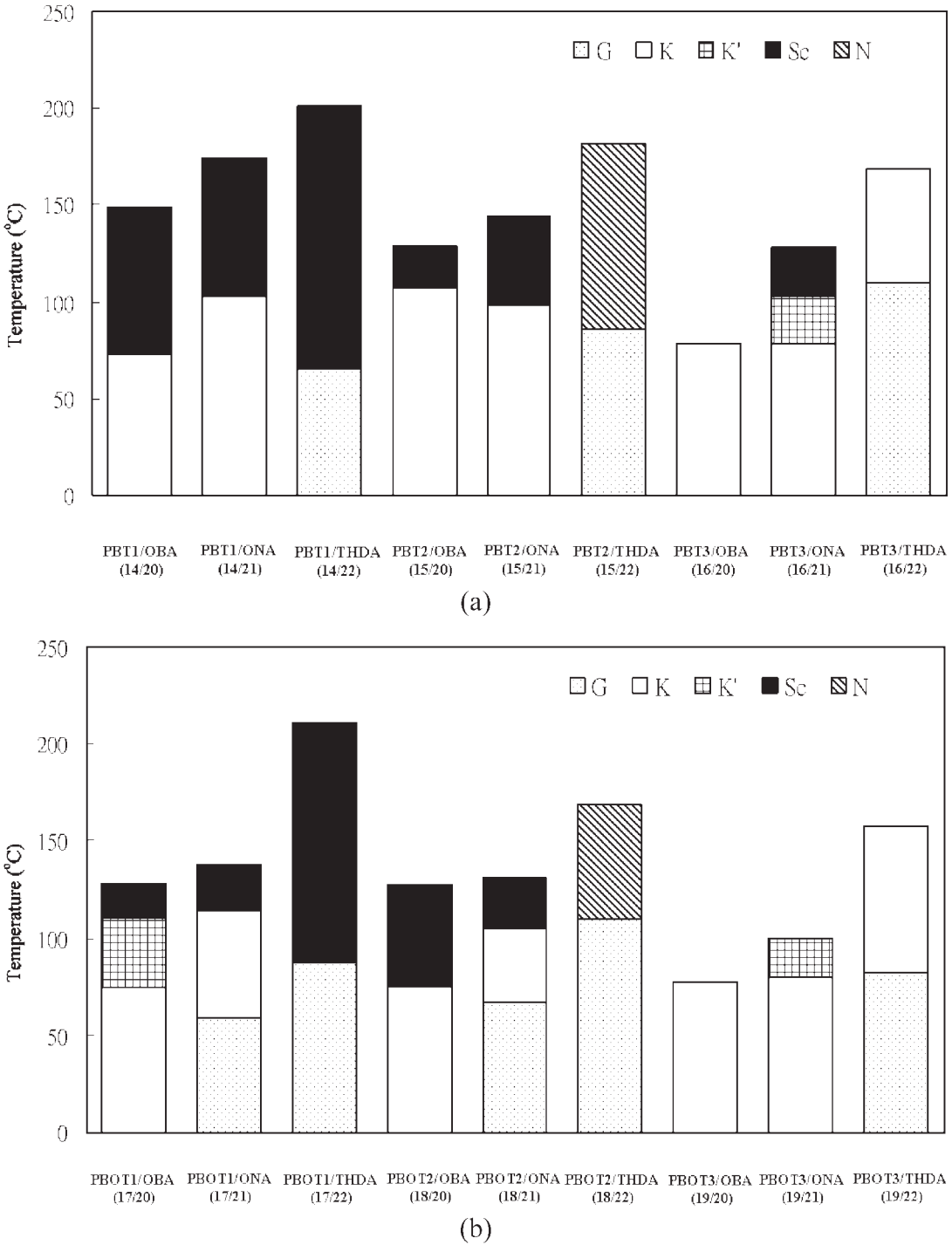

Figure 5. Phase diagrams (upon second heating) for (a) H-bonded polymer complexes of **PBT** and (b) H-bonded polymer complexes of **PBOT**.

supramolecular structures, three different H-donors, that is, two asymmetric monofunctional H-donors **OBA (20)** and **ONA (21)** along with one symmetric bifunctional H-donor **THDA (22)**, were utilized in the H-bonded side-chain/cross-linking polymers. These H-donors consist of three different rigid cores, such as phenylene, naphthalene, and thiophene groups, where **THDA (22)** containing a thiophene unit serves as a double H-donor (kinked H-bonded cross-linker). Some or

Table 2. Thermal Properties of H-Bonded Polymer Complexes[a,b]

H-Bonded Polymer Complex	Heating	Cooling
PBT1/OBA (14/20)	K 72.7 (2.0) Sc 149.1 (3.3) I	I 145.5 (−3.1) Sc 67[c] K
PBT1/ONA (14/21)	K 102.4 (3.96) Sc 174.2 (7.79) I	I 171.5 (−8.06) Sc 91[c] K
PBT1/THDA (14/22)	G 65.4 Sc 200.8 (6.21) I	I 174.9 (−5.83) K
PBT2/OBA (15/20)	K 107.3 (1.71) Sc 129[c] I	I 124[c] Sc 105.7 (−1.53) K
PBT2/ONA (15/21)	K 97.8 (1.21) Sc 143.9 (1.54) I	I 141.4 (−1.68) Sc 91[c] K
PBT2/THDA (15/22)	G 85.8 N 181.6 (7.1) I	I 180[c] N 82.1 (−6.85) G
PBT3/OBA (16/20)	K 78.1(3.6) I	I 72[c] K
PBT3/ONA (16/21)	K 78.1 (1.55) K′ 102.9 (2.3) I	I 96[c] K
PBT3/THDA (16/22)	G 109.3 K 168.6 (2.3) I	I 159[c] K 106.6 G
PBOT1/OBA (17/20)	K 74.2 (0.7) K′ 110.7 (3.24) Sc 127.7 (0.07) I	I 120.3 (−0.06) Sc 108.3 (−3.13) K
PBOT1/ONA (17/21)	G 58.8 K 114.1 (1.85) Sc 138.0 (2.83) I	I 133.1 (−2.51) Sc 106.3 (−0.91) K′ 83.5 (−1.11) K
PBOT1/THDA (17/22)	G 87.1 Sc 211.2 (5.7) I	I 195[c] Sc 86.3 G
PBOT2/OBA (18/20)	K 75.4 (1.75) Sc 127.3 (0.06) I	I 120.8 (−0.05) Sc 62.1 (−2.06) K
PBOT2/ONA (18/21)	G 66.6 K 105.4 (2.15) Sc 131.2 (3.85) I	I 127[c] Sc 103.9 (−2.15) K′ 79.6 (−1.64) K
PBOT2/THDA (18/22)	G 109.8 N 168.6 (3.4) I	I 157[c] N 105.8 G
PBOT3/OBA (19/20)	K 77.5 (3.9) I	I 60.2 (−3.2) K
PBOT3/ONA (19/21)	K 79.4 (−1.7)K′ 99.5 (2.0) I	I 90[c] K
PBOT3/THDA (19/22)	G 82.3 K 157[c] I	I 148[c] K 78.2 G

[a] Transition temperatures (°C) and enthalpies (in parentheses, kJ/mol) were determined by DSC at the second heating and cooling scans with a rate of 10 °C/min.
[b] G, glassy state; K, crystalline; Sc, smectic C; N, nematic; I, isotropic.
[c] The phase transition temperatures were obtained from POM.

emitters through H-bonds. H-bonded polymer complexes in Figure 5 and Table 2 exhibit melting temperatures (T_m) but without T_g, indicating their crystalline nature. In contrast to the nematic phase of pure H-acceptor polymers **PBT1-PBT2 (14–15)** and **PBOT1-PBOT2 (17–18)**, the smectic phase is introduced in their corresponding H-bonded polymer complexes due to the extended H-bonded mesogens by the combined rigid cores of H-donors. However, the nematic phase is recovered in the H-bonded cross-linking polymers composed of double H-donor **THDA (22)** and H-acceptor copolymers with a medium concentration of **CAZ** units, that is, **PBT2/THDA (15/22)** and **PBOT2/THDA (18/22)**, where the rod–rod interactions of H-bonded mesogens are reduced due to the dilution effect from the copolymerization of **CAZ** units in H-acceptor copolymers **PBT2 (15)** and **PBOT2 (18)**. In addition, due to the nonmesomorphic property of H-acceptor polymers **PBT3 (16)** and **PBOT3 (19)**, no mesomorphism is observed in all H-bonded polymer complexes containing H-acceptor copolymers **PBT3 (16)** and **PBOT3 (19)** with the highest concentration of **CAZ** units.

Comparing the phase transition temperatures of the H-bonded polymer counterparts containing different H-donors **OBA (20)**, **ONA (21)**, and **THDA (22)**, it demonstrates that longer and more rigid H-bonded structures will have higher isotropization temperatures (T_i), that is, H-bonded polymer complexes containing **THDA (22)** > those containing **ONA (21)** > those containing **OBA (20)**. For example, the T_i values of analogous H-bonded polymer complexes are in the order of **PBT1/THDA (14/22)** > **PBT1/ONA (14/21)** > **PBT1/OBA (14/20)**, that is, 200.8 °C, 174.2 °C, and 149.1 °C, respectively. Moreover, comparing analogous H-bonded polymer complexes consisting of the same H-acceptor polymers, the highest isotropization temperatures (Ti) and the broadest mesophasic ranges were observed in the supramolecular cross-linking polymers containing double H-donor **THDA (22)**. For instance, the H-bonded polymer networks **PBT1/THDA (14/22)** and **PBOT1/THDA (17/22)**, where double H-donor **THDA (22)** acts as H-bonded cross-linkers (acceptor:donor = 2:1) have the highest T_i values and the broadest smectic phase ranges in the analogues of H-bonded

polymer complexes, respectively. In general, the phase transition temperatures of H-bonded side-chain/cross-linking polymers will be enhanced while the H-bonded central cores are longer and more rigid.

Interestingly, by increasing the molar ratios of **CAZ** units in the H-bonded polymer networks, the smectic phase disappears but the nematic phase forms in **PBT2/THDA (15/22)** and **PBOT2/THDA (18/22)**, which is attributed to the **CAZ** segments in H-bonded polymer complexes **PBT2/THDA (15/22)** and **PBOT2/THDA (18/22)** (containing **PBT2 (15)** and **PBOT2 (18)** with a medium concentration of **CAZ** segments, c.a. 40% molar ratio) eliminate the layered arrangement of the H-bonded smectogens. However, in contrast to the nematic phase in supramolecular cross-linking polymers **PBT2/THDA (15/22)** and **PBOT2/THDA (18/22)**, supramolecular side-chain polymers **PBT2/OBA-PBT2/ONA (15/20–15/21)** and **PBTO2/OBA-PBOT2/ONA (18/20–18/21)** containing **PBT2 (15)** and **PBOT2 (18)** maintain the smectic phase, which are originated from the stronger π–π interactions of linear rods in the more linear H-bonded side-chain structures with pendent H-donors **OBA (20)** and **ONA (21)** rather than the weaker rod–rod interactions in the more kinked cross-linking structures with double H-donor **THDA (22)**. Furthermore, the mesophases even disappear in all H-bonded polymer complexes containing H-acceptor polymers **PBT3 (16)** and **PBOT3 (19)** due to the most concentrated **CAZ** segments in copolymers **PBT3 (16)** and **PBOT3 (19)** (with the highest concentration of **CAZ** segments, c.a. 70% molar ratio), which destroy the mesophasic arrangements completely. Besides, compared with **PBT2/OBA (15/20)** and **PBT2/ONA (15/21)**, analogous supramolecular side-chain polymers **PBT1/OBA (14/20)** and **PBT1/ONA (14/21)** containing H-acceptor homopolymer **PBT1** (without **CAZ** units) have higher T_i values (i.e., 149.1 and 174.2 °C higher than 129 and 143.9 °C, respectively) and broader smectic phase ranges (i.e., 76.4 and 71.8 °C broader than 21.7 and 46.1 °C, respectively). Similar trends of reduction in T_i values occur for supramolecular crosslinking polymers as increasing **CAZ** contents in the H-acceptor polymers. Hence, it is demonstrated that the mesophasic ranges and T_i values of these H-bonded polymer complexes are apparently reduced with increasing **CAZ** contents in the H-acceptor polymers.

In terms of lateral substitutions, the lateral methoxy groups in the H-bonded polymer complexes containing H-acceptor homopolymer **PBT1** are larger than the lateral methyl groups in the H-bonded polymer complexes containing H-acceptor homopolymer **PBOT1** to hinder the molecular packing, and thus to cause the reduction of the mesophases and T_i values prominently. For instance, in contrast to **PBT1/OBA (14/20)** and **PBT1/ONA (14/21)** containing H-acceptor homopolymer **PBT1** (with lateral methyl groups), analogous H-bonded polymer complexes **PBTO1/OBA (17/20)** and **PBOT1/ONA (17/21)** containing H-acceptor homopolymer **PBOT1** (with lateral methoxy groups) have lower T_i values (i.e., 127.7 and 138.0 °C lower than 149.1 and 174.2 °C, respectively) and narrower smectic phase ranges (i.e., 17.0 and 23.9 °C narrower than 76.4 and 71.8 °C, respectively). Thus, the steric effect plays an important role on the mesomorphic and thermal properties, where the larger lateral substitution may be detrimental to the molecular packing as well as the mesophasic ranges and T_i values. Above all, by utilization of H-acceptor polymers (mainly possess the nematic phase), various mesomorphic properties as shown in Figure 6 can be introduced to the H-bonded polymer complexes, including H-bonded side-chain/crosslinking polymers complexed with asymmetric monofunctional and symmetric bifunctional H-donors. The smectic and nematic phases in the H-bonded polymer complexes were not only identified by POM but also could further be confirmed by XRD measurements.

X-Ray Diffraction Analysis

To elucidate the structure of the mesophases, XRD measurements were accomplished at the temperature ranges of mesophases for all H-bonded polymer complexes (see Table 3). To prove the formation of the supramolecular structures, the smectic layer arrangements can be characterized to evaluate the H-bonded architectures. However, the calculations of tilt angles by Chemoffice in Table 3 did not consider their Van der Waals radii. Moreover, the measurements of the lengths for the H-bonded complexes were made in the rigid and all-trans conformations, which might be not exactly what occur in the mesophases, so the theoretical molecular lengths and tilt angles presented here are only rough estimates. Based on the theoretical geometries estimated by CS Chem-Office, the molecular lengths of H-bonded polymer complexes **PBT1/OBA (14/20)**, **PBT1/ONA (14/21)**, and **PBT1/THDA (14/22)** are 55.7, 58.1,

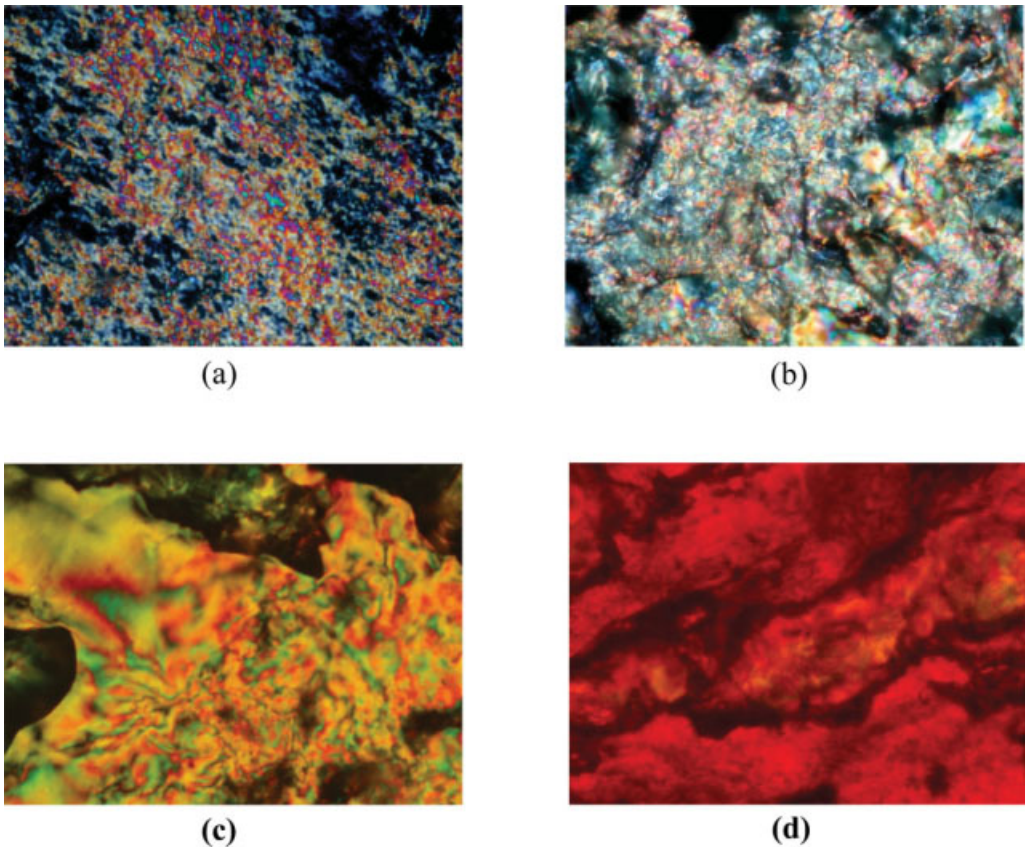

Figure 6. Liquid crystalline textures of H-bonded polymer complexes observed by POM (a) the Sc phase in **PBT1/ONA (14/21)** at 160 °C (cooling), (b) the Sc phase in **PBT2/ONA (15/21)** at 110 °C (cooling), (c) the nematic phase in **PBT2/THDA (15/22)** at 180 °C (cooling), (d) the Sc phase in **PBOT1/THDA (17/22)** at 160 °C (cooling).

Table 3. The *d*-Spacing and Tilt Angle Values of the Sc Phase in H-Bonded Polymer Complexes

H-Bonded Polymer Complex	Phase	Measured *d* Spacing (Å) (Cooling)	Theoretical Molecular Length (Å)[a]	Tilt Angle (°)
PBT1/OBA (14/20)	Sc	46.9 (130 °C)	55.7	32.7
PBT1/ONA (14/21)	Sc	50.1 (160 °C)	58.1	30.4
PBT1/THDA (14/22)	Sc	61.8 (165 °C)	75.4	35.0
PBT2/OBA (15/20)	Sc	42.2 (130 °C)	55.7	40.7
PBT2/ONA (15/21)	Sc	50.3 (110 °C)	58.1	30.0
PBT2/THDA (15/22)	N[b]	–	–	–
PBOT1/OBA (17/20)	Sc	49.3 (115 °C)	55.7	27.7
PBOT1/ONA (17/21)	Sc	50.0 (120 °C)	58.1	30.6
PBOT1/THDA (17/22)	Sc	63.0 (160 °C)	75.4	33.3
PBOT2/OBA (18/20)	Sc	43.0 (120 °C)	55.7	39.5
PBOT2/ONA (18/21)	Sc	46.9 (120 °C)	58.1	36.2
PBOT2/THDA (18/22)	N[b]	–	–	–

[a] The theoretical molecular lengths of H-bonded polymer complexes were estimated by the sum of molecular projection lengths of the H-bonded components along the rigid cores through molecular modeling.
[b] Nematic phase was observed by POM and confirmed by XRD (no layer *d*-spacing peaks).

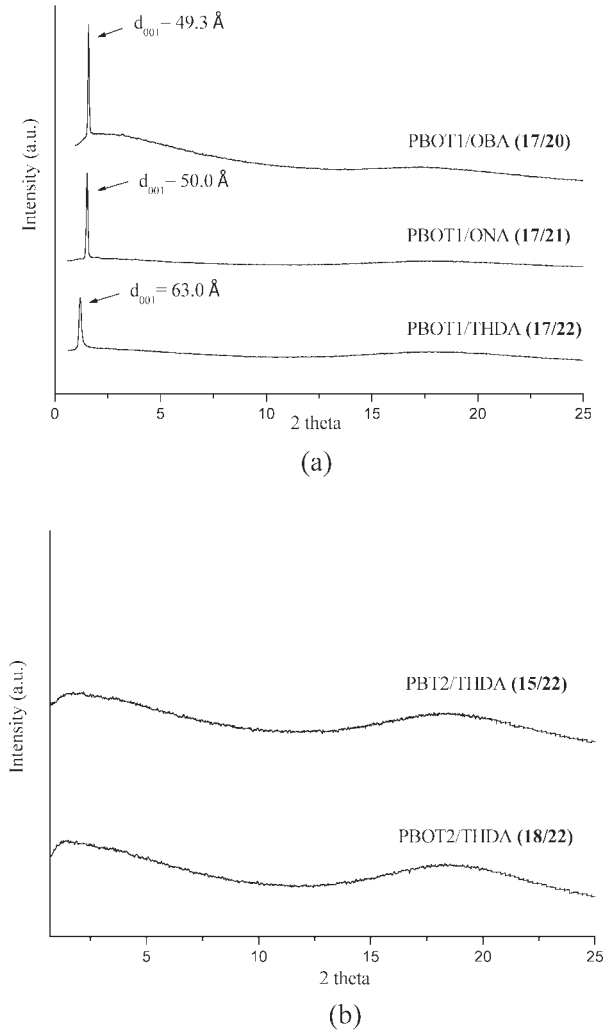

Figure 7. X-ray diffraction patterns of H-bonded polymer complexes (a) the Sc phase in **PBOT1/OBA (17/20)** at 115 °C, **PBOT1/ONA (17/21)** at 120 °C, and **PBOT1/THDA (17/22)** at 160 °C; (b) the nematic phase in **PBT2/THDA (15/22)** and **PBOT2/THDA (18/22)** at 130 °C.

and 75.4 Å, respectively, which are calculated from the molecular projection lengths of the fully extended molecular lengths along the rigid cores. As shown in Table 3 and Figure 7(a), the XRD patterns of H-bonded polymer complexes **PBOT1/OBA (17/20)**, **PBOT1/ONA (17/21),** and **PBOT1/THDA (17/22)** indicate that the layer *d*-spacing values at 115, 120, and 160 °C are 49.3, 50.0, and 63.0 Å, respectively. In general, the XRD data demonstrate the *d*-spacing values at different temperatures, from which the individual tilt angles can be estimated. According to these findings in XRD experiments, the tilt angles of are 27.7°, 30.6°, and 33.3°, respectively, as H-acceptor polymer **PBOT1 (17)** was H-bonded to H-donors **OBA (20)**, **ONA (21)**, and **THDA (22)**. These results support that most H-bonded polymer complexes are suitable to be identified as the tilted smectic C phase by XRD measurements, and their tilt angles in Table 3 can be calculated from the theoretical molecular model. In contrast to the longer (even though kinked) doubly H-bonded rods of supramolecular cross-linking polymers containing bifunctional H-donor **THDA (22)** (as a H-bonded cross-linker), the supramolecular side-chain polymers containing monofunctional H-donors **OBA (20)** and **ONA (21)** always have smaller *d*-spacing values due to their shorter singly H- bonded rods. Moreover, compared with **OBA (20)**, H-donor **ONA (21)** possesses a longer rigid naphthyl group, so the *d*-spacing values of the H-bonded polymer complexes containing **ONA (21)** will be a little longer (c.a. 2.4 Å) in contrast to those containing **OBA (20)**. Regarding the H-bonded polymer complexes containing H-acceptor polymers with different contents of **CAZ** units in Table 3, it is interesting that all *d*-spacing values of H-bonded polymer complexes bearing H-acceptor homopolymers **PBT1 (14)** and **PBOT1 (17)** (without **CAZ** units) are larger than those bearing H-acceptor copolymers **PBT2 (15)** and **PBOT2 (18)** bearing **CAZ** units, respectively. As described previously, the **CAZ** segments reduce the molecular packing of smectogens, so the smaller *d*-spacing values are induced by that the smectic layers are more disordered and the pendent mesogens are separated (and diluted) by **CAZ** units. Furthermore, the lack of small angle XRD patterns (for smectogens) in the mesophase of H-bonded polymer complexes **PBT2/THDA (15/22)** and **PBOT2/THDA (18/22)** support the existence of the nematic phase [see Fig. 7(b)]. As shown in Figure 8, the diffraction patterns of H-bonded polymer complex **PBT1/ONA (14/21)** indicate the diffraction peak is increased upon cooling from the isotropic phase (180 °C) to the crystalline state (50 °C), so the layer *d*-pacing value (in the inset of Fig. 8) reduces from 50.1 Å (at 160 °C) to 49.7 Å (at 120 °C), which could be due to the increase of tilt angle by decreasing temperature. The disappearance of small-angle diffraction peak at 180 °C indicates the absence of the layered smectic structure in the isotropic phase.

Optical Properties

The absorption and PL spectral data of all luminescent H-acceptor polymers **PBT1-PBT3 (14–**

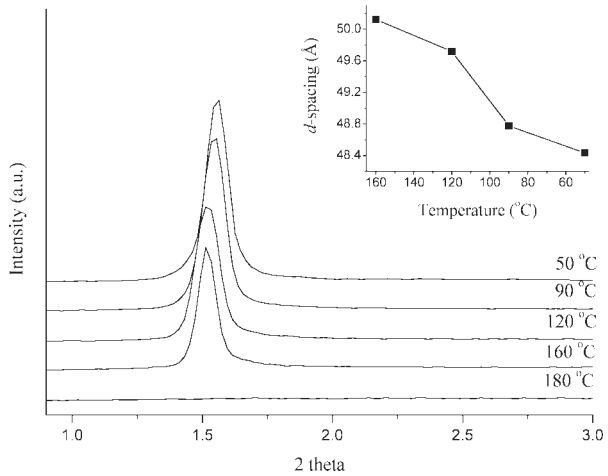

Figure 8. X-ray diffraction patterns for H-bonded polymer complex **PBT1/ONA (14/21)** upon cooling from the isotropic phase (180 °C) to solid (50 °C).

16) and **PBOT1-PBOT3 (17–19)** (in both THF solutions and solid films) as well as all H-bonded polymer complexes (in solid films) are summarized in Tables 4–5. The PL quantum yields (Φ_{PL}) of polymers **PBT1-PBT3 (14–16)** and **PBOT1-PBOT3 (17–19)** in solutions were excited at the maximum absorption peak as listed in Table 4. As shown in Figure 9(a), the maximum absorption peaks of **PBT** and **PBOT** series are 350 and 384 (322) nm, respectively. The absorption bands of **PBT1-PBT3 (14–16)** in THF solutions at c.a. 294, 330, and 344 nm are originated from the combined absorption bands of **CAZ** pendent groups. The additional absorption bands of polymers **PBOT1-PBOT3 (17–19)** at 320–322 nm are assigned to the n–π^* transition[43] contributed from the lateral methoxy groups in conjugated chromophores. Similarly, **PBOT1-PBOT3 (17–19)** have

Table 4. Absorption and Photoluminescence Spectral Data of H-Acceptor Polymers

H-Acceptor Polymer	$\lambda_{abs,sol}$[a] (nm)	$\lambda_{PL,sol}$[a] (nm)	$\lambda_{PL,film}$ (nm)	$\Phi_{PL,sol}$[b] (%)
PBT1 (14)	350	440	487	40
PBT2 (15)	345	435	479	51
PBT3 (16)	344	431	471	59
PBOT1 (17)	322,384	449	494	49
PBOT2 (18)	320,384	447	492	56
PBOT3 (19)	320,382	445	485	63

[a] Absorption and PL emission spectra were recorded in dilute THF solutions at room temperature.
[b] PL quantum yield in THF and 9,10-diphenylanthrance is the reference of quantum yield.

Table 5. Photophysical Properties of H-Acceptor Polymers and H-Bonded Polymer Complexes in Solid Films

H-Acceptor Polymer or H-Bonded Polymer Complex	$\lambda_{PL,sol}$ (nm)	$\lambda_{PL,film}$ (nm)	$\Delta\lambda_{PL,film}$[a] (nm)
PBT1 (14)	440	487	–
PBT1/OBA (14/20)		517	30
PBT1/ONA (14/21)		521	34
PBT1/THDA (14/22)		565	78
PBT2 (15)	435	479	–
PBT2/OBA (15/20)		512	33
PBT2/ONA (15/21)		514	35
PBT2/THDA (15/22)		553	74
PBT3 (16)	431	471	–
PBT3/OBA (16/20)		505	34
PBT3/ONA (16/21)		511	40
PBT3/THDA (16/22)		546	75
PBOT1 (17)	449	494	–
PBOT1/OBA (17/20)		543	49
PBOT1/ONA (17/21)		542	48
PBOT1/THDA (17/22)		587	93
PBOT2 (18)	447	492	–
PBOT2/OBA (18/20)		535	43
PBOT2/ONA (18/21)		537	45
PBOT2/THDA (18/22)		582	90
PBOT3 (19)	445	485	–
PBOT3/OBA (19/20)		536	51
PBOT3/ONA (19/21)		534	49
PBOT3/THDA (19/22)		571	86

[a] The difference of PL emissions between the H-acceptor polymer and its H-bonded polymer complex.

the same tendency by increasing the content of **CAZ** units. In Figure 9(b), the PL spectra of H-acceptor polymers **PBT1-PBT3 (14–16)** emitted blue light c.a. 431–440 nm in THF solutions. In comparison with luminescent homopolymer **PBT1 (14)**, the slightly blue-shifted PL spectra of copolymers **PBT2** and **PBT3 (15** and **16)** can be explained by the dilution effect of the incorporated **CAZ** units to reduce the aggregation of the pyridyl chromophores, which also can enhance PL quantum yields (Φ_{PL} = 40–59%) by copolymerization with **CAZ** units. Correspondingly, similar blue-shifted PL spectra ($\lambda_{PL,sol}$ = 445–449 nm) and enhanced PL quantum yields (Φ_{PL} = 49–63%) were observed in THF solutions of analogous H-acceptor polymers **PBOT2-PBOT3 (18–19** with lateral methoxy groups**)** due to the dilution effects of **CAZ** units in copolymers. Furthermore, in contrast to polymers **PBT1-PBT3 (14–16)**, polymers **PBOT1-PBOT3 (17–19)** have more red-shifted PL emissions due to the stronger electron

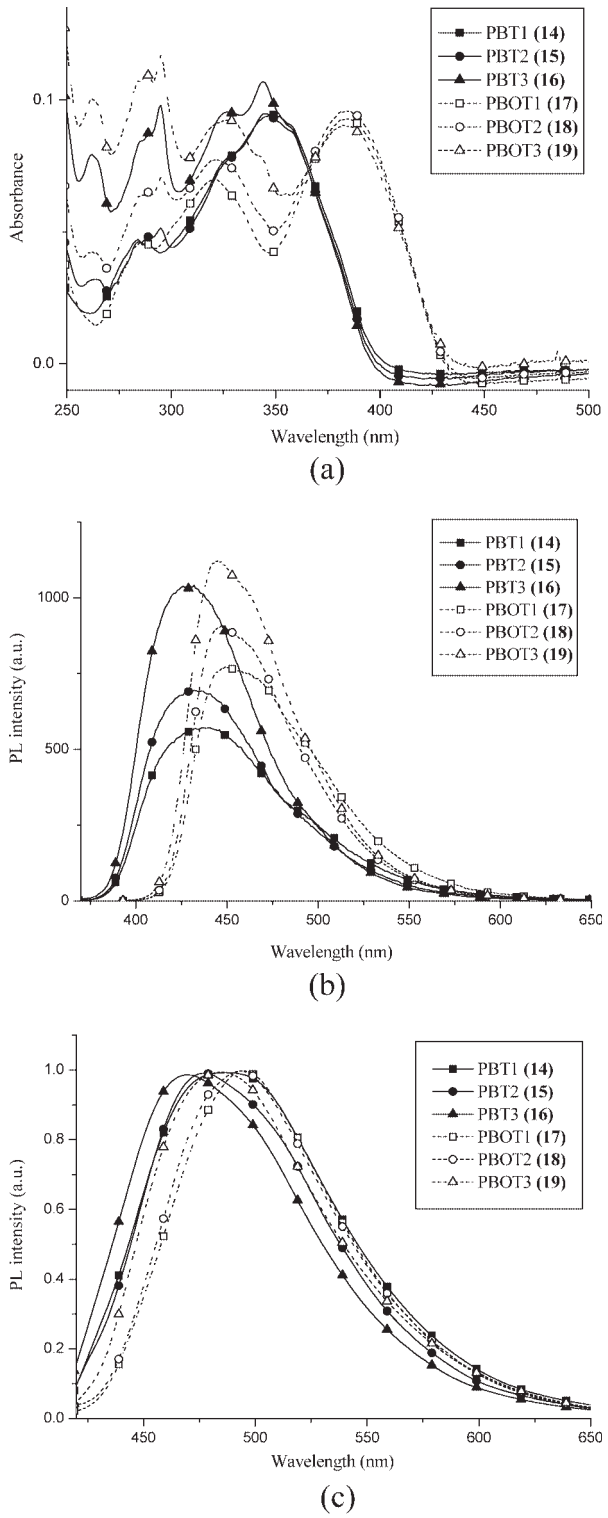

Figure 9. (a) Absorption spectra, (b) PL spectra (excited at the maximum absorption wavelengths) in THF solutions, (c) normalized PL spectra (excited at the maximum absorption wavelengths) of H-acceptor polymers **14–19** in solid films.

donating effect of lateral methoxy groups, which induce smaller energy band gaps in chromophores. In Figure 9(c), comparing polymers **PBT1-PBT3 (14–16** with lateral methyl groups**)** and **PBOT1-PBOT3 (17–19** with lateral methoxy groups**)**, the PL spectra in solid films are more red-shifted than those in THF solutions, which indicate that more serious π–π stacking and molecular aggregation occur in solid films. Additionally, due to the larger separation of chromophores by the larger size of lateral methoxy groups in **PBOT1-PBOT3 (17–19)**, they have higher PL quantum yields (Φ_{PL} = 49–63%) than **PBT1-PBT3 (14–16)** with lateral methyl groups (Φ_{PL} = 40–59%), respectively.

As shown in Table 5, the H-donor acids play an important role to induce the PL emission shift of light-emitting H-acceptor polymers in H-bonded polymer complexes because of their different acidities being able to tune the emission colors (λ_{max}) by H-bonds. The proton donors in the H-bonded polymer complexes do not have PL properties due to lacking of conjugated structures, so they only offer the solid solvent environments with different pKa values [**OBA (20)**: pKa $\sim$ 4.21: **ONA (21)**: pKa $\sim$ 4.17; **THDA (22)**: pKa $\sim$ 3.49]. Thus, different degrees of H-bonding occur in H-bonded polymer complexes for various acids H-bonded with light-emitting H-acceptor polymers, that is, different electron densities and energy band-gaps of light-emitting H-bonded polymer complexes are induced by the H-bonding of distinct solid H-donors. In Table 5, compared with H-acceptor polymers **PBT1-PBT3 (14–16)**, their H-bonded polymer complexes can generate 30–40 nm of red-shifted PL emissions in λ_{max} as H-bonded to the asymmetric monofunctional H-donors **OBA (20)** and **ONA (21)**, and up to 74–78 nm of red-shifted PL emissions in λ_{max} as H-bonded to the symmetric bifunctional H-donor **THDA (22)**. The redder-shifted PL emissions are originated from the stronger H-bonded effect of H-donor acids with smaller pKa values and thus to generate stronger H-bonding in corresponding H-bonded polymer complexes. Similarly, the PL emission peaks of the H-bonded polymer complexes containing H-acceptor polymers **PBOT1-PBOT3 (17–19)** are red-shifted about 43–51 nm as complexed with **OBA (20)** and **ONA (21)**, and red-shifted 86–93 nm as complexed with **THDA (22)**. For instance, compared with H-acceptor polymers **PBT2 (15)** and **PBOT2 (18)**, different extents of red-shifted PL emissions occurred in solid films of their H-bonded polymer complexes **PBT2/OBA-PBT2/**

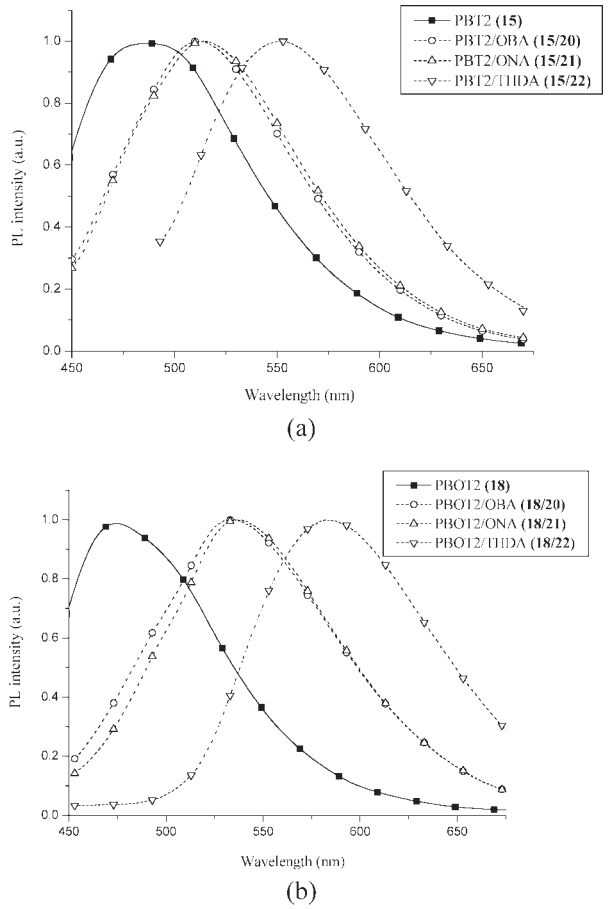

Figure 10. Normalized PL spectra (excited at the maximum absorption wavelengths) of (a) H-acceptor polymer **PBT2 (15)** and its H-bonded polymer complexes **PBT2/OBA (15/20), PBT2/ONA (15/21)**, and **PBT2/THDA (15/22)** in solid films; (b) H-acceptor polymer **PBOT2 (18)** and its H-bonded polymer complexes **PBOT2/OBA (18/20), PBOT2/ONA (18/21)**, and **PBOT2/THDA (18/22)** in solid films.

THDA (15/20–15/22) and **PBOT2/OBA-PBOT2/THDA (18/20–18/22)** (were excited at the maximum absorption wavelengths) in Figure 10. In general, by decreasing pKa values of proton donors, more red-shifted wavelengths of PL emissions of H-bonded polymer complexes were observed. In comparison with H-bonded polymer complexes containing **PBT1**-**PBT3 (14–16)**, those containing H-acceptor polymers **PBOT1**-**PBOT3 (17–19)** possess larger red-shifted PL emissions by the formation of H-bonded polymer complexes due to their stronger electron donating effect of lateral methoxy groups. Besides, H-bonded polymer complexes containing H-acceptor polymers with different **CAZ** contents appear to have similar degrees of red-shifted PL emissions in analogous H-bonded polymer complexes. Hence, the pKa values of H-donors are more important than the steric effect of **CAZ** contents in the H-bonded polymer complexes. Consequently, the results demonstrate that more red-shifted PL emissions happen in the H-bonded polymer complexes as H-donors with smaller pKa values are H-bonded to the light-emitting H-acceptor polymers. Therefore, PL emission colors, that is, λ_{max} values, of H-bonded polymer complexes can be tuned not only by adjusting the light-emitting conjugated pyridyl cores but also by changing the nonemitting H-donors with different pKa values.

CONCLUSIONS

In conclusion, H-donors (asymmetric monofunctional H-donors and symmetric bifunctional H-donor) and H-acceptor polymers were utilized to control the mesomorphic and PL properties effectively by the concept of supramolecular architecture. The H-acceptor copolymers were composed of different molar ratios of pendent *N*-vinylcarbazole units and light-emitting H-acceptor groups randomly to increase the glass transition temperatures and to reduce the π-π stacking of the conjugated H-acceptor chormorphores in the copolymers as well as in their H-bonded polymer complexes. The supramolecular architectures of H-bonded side-chain/crosslinking polymers were also confirmed by FTIR and XRD measurements. They have distinct mesomorphism and phase transition temperatures related to their supramolecular structures with different nonlinearities and rigidities. The mesomorphic properties were changed from the nematic phase to the smectic C phase by the introduction of H-bonds to the supramolecular polymers, and then shifted to the nematic and nonmesophases by various H-donor acids and H-acceptor copolymers with corresponding supramolecular side-chain/crosslinking structures. In addition, the emission color of light-emitting H-acceptor polymers can be tuned by their surrounding nonemitting H-donors. Redder shifts in PL emissions were observed in the H-bonded supramolecules with H-donors having smaller pKa values.

The authors are grateful to the National Center for High-performance Computing for computer time and facilities. The powder XRD measurements are supported by beamline BL17A (charged by Jey-Jau Lee) of the National Synchrotron Radiation Research Center

(NSRRC), in Taiwan. The financial supports of this project provided by the National Science Council of Taiwan (ROC) through NSC 96-2113-M-009-015 and Chung-Shan Institute of Science and Technology (Taiwan) are acknowledged.

REFERENCES AND NOTES

1. (a) Lehn, J.-M. Supramolecular Chemistry, Concepts and Perspectives; VCH: Weinheim, 1995; (b) Lehn, J. M. Science 2002, 295, 2400–2403; (c) Ikkala, O.; ten Brinke, G. Science 2002, 295, 2407–2409; (d) Stupp, S. I.; Son, S.; Lin, H.-C.; Li, L.-S. Science 1993, 259, 59–63; (e) Ajayaghosh A.; Praveen, V. K. Acc Chem Res 2007, 40, 644–656.
2. (a) Wessendorf, F.; Gnichwitz, J.-F.; Sarova, G. H.; Hager, K.; Hartnagel, U.; Guldi, D. M.; Hirsch A. J Am Chem Soc 2007, 129, 16057–16071; (b) Nair, K. P.; Breedveld, V.; Weck, M. Macromolecules 2008, 41, 3429–3438; (c) Sievers, T. K.; Vergin, A.; Möhwald, H.; Kurth, D. G. Langmuir 2007, 23, 12179–12184; (d) Kim, J.-H.; Rahman, M. S.; Lee, J.-S.; Park, J.-W. Macromolecules 2008, 41, 3181–3189; (e) Nair, K. P.; Weck, M. Macromolecules 2007, 40, 211–219; (f) Nair, K. P.; Pollino, J. M.; Weck, M. Macromolecules 2006, 39, 931–940; (g) South, C. R.; Burd, C.; Weck, M. Acc Chem Res 2007, 40, 63–74; (h) Broeren, M. A. C.; Linhardt, J. G.; Malda, H.; de Waal, B. F. M.; Versteegen, R. M.; Meijer, J. T.; Löwik, D. W. P. M.; van Hest, J. C. M.; van Genderen, M. H. P.; Meijer, E. W. J Polym Sci Part A: Polym Chem 2005, 43, 6431–6437; (i) Montarnal, D.; Cordier, P.; Soulié-Ziakovic, C.; Tournilhac, F.; Leibler, L. J Polym Sci Part A: Polym Chem 2008, 46, 7925–7936; (j) Vellis, P. D.; Mikroyannidis, J. A.; Lo, C. N.; Hsu C. S. J Polym Sci Part A: Polym Chem 2008, 46, 7702–7712; (k) Cheng, C. C.; Huang, C. F.; Yen, Y. C.; Chang, F. C. J Polym Sci Part A: Polym Chem 2008, 46, 6416–6424; (l) Coluccini, C.; Metrangolo, P.; Parachini, M.; Pasini, D.; Resnati, G.; Righetti, P. J Polym Sci Part A: Polym Chem 2008, 46, 5202–5213; (m) Bosman, A. W.; Sijbesma, R. P. J Polym Sci Part A: Polym Chem 2008, 46, 3877–3885; (n) Aamer, K. A.; Tew, G. N. J Polym Sci Part A: Polym Chem 2007, 45, 1109–1121.
3. Kato, T.; Hirota, N.; Fujishima, A.; Fréchet, J. M. J. J Polym Sci Part A: Polym Chem 1996, 34, 57–62.
4. Kato, T.; Fréchet, J. M. J.; Wilson, P. G.; Saito, T.; Uryu, T.; Fujishima, A.; Jin, C.; Kaneuchi, F. Chem Mater 1993, 5, 1094–1100.
5. Kato, T.; Mizoshita, N.; Kishimoto, K. Angew Chem Int Ed Engl 2006, 45, 38–68.
6. Kumar, U.; Kato, T.; Fréchet, J. M. J. J Am Chem Soc 1992, 114, 6630–6639.
7. Kato, T.; Kihara, H.; Kumar, U.; Uryu, T.; Fréchet, J. M. J. Angew Chem Int Ed Engl 1994, 33, 1644–1645.
8. Kato, T.; Fréchet, J. M. J. Macromol Symp 1995, 98, 311–325.
9. Kato, T.; Fukumasa, M.; Fréchet, J. M. J. Chem Mater 1995, 368–372.
10. Gimeno, N.; Ros, M. B.; Serrano, J. L.; De la Fuente, M. R. Chem Mater 2008, 20, 1262–1271.
11. Vera, F.; Almuzara, C.; Orera, I.; Barberá, J.; Oriol, L.; Serrano, J. L.; Sierra, T. J Polym Sci Part A: Polym Chem 2008, 46, 5528–5541.
12. Ma, X. J.; Shen, Y. T.; Deng, K.; Tang, H.; Lei, S. B.; Wang, C.; Yang, Y. L.; Feng, X. Z. J Mater Chem 2007, 17, 4699–4704.
13. Xu, J.; Toh, C. L.; He, C. J Polym Sci Part A: Polym Chem 2008, 46, 4691–4703.
14. Burke, K. A.; Sivakova, S.; McKenzie, B. M.; Mather, P. T.; Rowan, S. J. J Polym Sci Part A: Polym Chem 2006, 44, 5049–5059.
15. Vera, F.; Tejedor, R. M.; Romero, P.; Barberá, J.; Ros, M. B.; Serrano, J. L.; Sierra, T. Angew Chem Int Ed Engl 2007, 46, 1873–1877.
16. Álvarez, L.; Barberá, J.; Puig, L.; Romero, P.; Serrano, J. L.; Sierra, T. J Mater Chem 2006, 16, 3768–3773.
17. Barberá, J.; Puig, L.; Romero, P.; Serrano, J. L.; Sierra, T. J Am Chem Soc 2006, 128, 4487–4492.
18. (a) Huang, W.; Han, C. D. Macromolecules 2006, 39, 4735–4745; (b) Huang, W.; Han, C. D. Macromolecules 2006, 39, 257–267.
19. (a) Lee, K. M.; Han, C. D. Polymer 2003, 44, 4573–4588; (b) Kim, S. S.; Han, C. D. Polymer 1994, 35, 93–103.
20. Xu, J.; Toh, C. L.; Liu, X.; Wang, S.; He, C.; Lu, X. Macromolecules 2005, 38, 1684–1690.
21. Toh, C. L.; Xu, J.; Liu, X.; Lu, X.; He, C. J Polym Sci Part A: Polym Chem 2005, 43, 4731–4743.
22. (a) Cui, L.; Dahmane, S.; Tong, X.; Zhu, L.; Zhao, Y. Macromolecules 2005, 38, 2076–2084; (b) Cui, L.; Zhao, Y. Chem Mater 2004, 16, 2076–2082.
23. (a) Aubertin, F.; Zhao, Y. J Polym Sci Part A: Polym Chem 2004, 42, 3445–3455; (b) Bo, Q.; Zhao, Y. J Polym Sci Part A: Polym Chem 2006, 44, 1734–1744.
24. Medvedev, A. V.; Barmatov, E. B.; Medvedev, A. S.; Shibaev, V. P.; Ivanov, S. A.; Kozlovsky, M.; Stumpe, J. Macromolecules 2005, 38, 2223–2229.
25. van Zoelen, W.; Alberda van Ekenstein, Z.; Ikkala, O.; ten Brinke, G. Macromolecules 2006, 39, 6574–6579.
26. Xu, J.; Liu, X.; Lin, T.; Huang, J.; He, C. Macromolecules 2005, 38, 3554–3557.
27. Hua, F.; Yang, X.; Gong, B.; Ruckenstein, E. J Polym Sci Part A: Polym Chem 2005, 43, 1119–1128.
28. Chen, Y. Y.; Tao, Y. T.; Lin, H. C. Macromolecules 2006, 39, 8559–8566.
29. Chen, Y. Y.; Lin, H. C. J Polym Sci Part A: Polym Chem 2007, 45, 3243–3255.

30. Lin, H. C.; Lin, Y. S.; Lin, Y. S.; Chen, Y. T.; Chao, I.; Li, T. W. Macromolecules 1998, 31, 7298–7311.
31. Burroughes, J. H.; Bradley, D. C.; Brown, A. R.; Marks, R. N.; Mackay, K.; Friend, R. H.; Burn, P. L.; Holmes, A. B. Nature 1990, 347, 539– 541.
32. Yang, Z.; Sokolik, I.; Karasz, F. E. Macromolecules 1993, 26, 1188–1190.
33. Hu, B.; Yang, Z.; Karasz, F. E. J Appl Phys 1994, 76, 2419–2422.
34. Wang, G.; Yuan, C.; Wu, H.; Wei, Y. J Appl Phys 1995, 78, 2679–2683.
35. Romero, D. B.; Schaer, M.; Zuppiroli, L.; Leclerc, M.; Adès, D.; Siove, A. Synth Met 1996, 80, 271–277.
36. Lin, H. C.; Tsai, C. M.; Huang, G. H.; Tao, Y. T. Macromolecules 2006, 39, 557–568.
37. Wu, C. W.; Lin, H. C. Macromolecules 2006, 39, 7985–7997.
38. Lin, H. C.; Sheu, H. Y.; Chang, C. L.; Tsai, C. J Mater Chem 2001, 11, 2958–2965.
39. Yang, P. J.; Wu, C. W.; Sahu, D.; Lin, H. C. Macromolecules 2008, 41, 9692–9703.
40. Eaton, D. Pure Appl Chem 1998, 60, 1107–1114.
41. Cui, L.; Lattermann, G. Macromol Chem Phys 2002, 203, 2432–2437.
42. Lee, J. Y.; Painter, P. C.; Coleman, M. M. Macromolecules, 1988, 21, 954–960.
43. Sun, Y. P.; Ma, B.; Bunker, C. E. J Phys Chem A 1998, 102, 7580–7590.